Inorganic Chemistry

Article

pubs.acs.org/IC

Manganese(II) Complexes with the Non-steroidal Anti-Inflammatory Drug Tolfenamic Acid: Structure and Biological Perspectives

Marianthi Zampakou,[†] Natalia Rizeq,[†] Vassilis Tangoulis,[†] Athanasios N. Papadopoulos,[‡] Franc Perdih,[§] Iztok Turel,[§] and George Psomas*,[†]

[†]Department of General and Inorganic Chemistry, Faculty of Chemistry, Aristotle University of Thessaloniki, GR-54124 Thessaloniki, Greece

[‡]Department of Nutrition and Dietetics, Faculty of Food Technology and Nutrition, Alexandrion Technological Educational Institution, Sindos, Thessaloniki, Greece

[§]Faculty of Chemistry and Chemical Technology, University of Ljubljana, Askerceva 5, 1000 Ljubljana, Slovenia

Supporting Information

ABSTRACT: Manganese(II) complexes with the non-steroidal anti-inflammatory drug tolfenamic acid (Htolf) with the nitrogen-donor heterocyclic ligands 1,10-phenanthroline (phen), pyridine (py), or 2,2′-bipyridylamine (bipyam) and/or the oxygen-donor ligands H_2O or *N*,*N*-dimethylformamide (DMF) have been synthesized and characterized. The crystal structures of complexes $[Mn(tolf\text{-}O)(tolf\text{-}O,O')(phen)(H_2O)]$, $[Mn_2(\mu_2\text{-}tolf\text{-}O,O')_2(tolf\text{-}O,O')_2(bipyam)_2]$, $[Mn_2(\mu_2\text{-}H_2O)(\mu_2\text{-}tolf\text{-}O,O')_2(tolf\text{-}O)_2(py)_4]\cdot 1.5MeOH\cdot py$, and $[Mn(\mu_2\text{-}tolf\text{-}O,O')_2(DMF)_2]_n$ have been determined by X-ray crystallography. The interaction of the complexes with serum albumin proteins was investigated, and relative high binding constant values were calculated. The ability of the compounds to scavenge 1,1-diphenyl-picrylhydrazyl, 2,2′-azinobis(3-ethylbenzothiazoline-6-sulfonic acid), and hydroxyl radicals was evaluated, and $[Mn(tolf)_2(phen)(H_2O)]$ was the most active scavenger among the compounds. The compounds have also exhibited noteworthy *in vitro* inhibitory activity against soybean lipoxygenase. UV titration studies of the interaction of the complexes with calf-thymus (CT) DNA have proved the binding to CT DNA with $[Mn(\mu_2\text{-}tolf)_2(DMF)_2]_n$ exhibiting the highest DNA-binding constant (K_b = 5.21 (±0.35) × 10^5 M^{-1}). The complexes bind to CT DNA probably via intercalation as suggested by DNA-viscosity measurements and competitive studies with ethidium bromide (EB), which revealed the ability of the complexes to displace the DNA-bound EB.

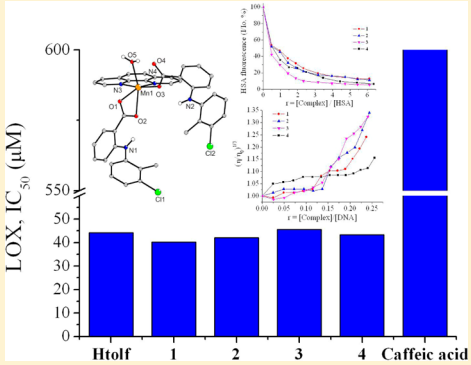

1. INTRODUCTION

Manganese is considered a significant biometal; Mn is located in the active center of a plethora of enzymes,[1−3] and manganese-containing compounds such as SC-52608, an anticancer agent, and Teslascan, an MRI contrast agent, are used in medicine.[4] Furthermore, manganese complexes with diverse ligands have already exhibited bactericidal,[5,6] antiproliferative,[7−9] and fungicidal[10] activity, and the study of the bioactiviy of novel Mn complexes is of increasing interest.

The side-effects of the non-steroidal anti-inflammatory drugs (NSAIDs) are well-known and thoroughly studied;[11] therefore, NSAIDs are common antipyretic, analgesic, and anti-inflammatory drugs in clinical use. The main known action of the NSAIDs is the inhibition of the prostaglandins production mediated by cyclo-oxygenase (COX).[12] The antitumor activity of NSAIDs has been attributed to synergism with antitumor drugs in clinical use,[13] to COX-independent mechanisms[14] and to apoptosis via caspase activation[15] or via mechanisms with the involvement of free radicals.[16,17] To investigate the anti-inflammatory and potential anticancer activity of the NSAIDs and their complexes, the study of the antioxidant properties and the DNA interaction is of expanding interest and great importance and needs further evaluation because the existing number of relevant reports is rather limited.[18,19] Additionally, only one manganese complex bearing NSAIDs as ligands has been structurally characterized and reported in the literature, i.e., the manganese(II) complex of niflumic acid.[20]

Tolfenamic acid (Htolf, Scheme 1) is a NSAID of the *N*-phenylanthranilic acid derivatives and is similar to other fenamates (e.g., mefenamic acid, flufenamic acid) in clinical use.[21] As a drug, Htolf is an antipyretic, antirheumatoid, and

Scheme 1. Tolfenamic Acid

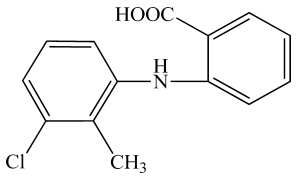

Received: October 8, 2013
Published: January 27, 2014

   dx.doi.org/10.1021/ic4025487 | *Inorg. Chem.* 2014, 53, 2040−2052

anti-inflammatory and is also administered for veterinary purposes.[22] The crystal structures of tin(IV),[23] copper(II),[24] cobalt(II),[25] and zinc(II)[26] complexes of tolfenamic acid have already been reported in the literature.

In our recent reports, we have focused on the interaction of NSAIDs containing a carboxylate group with diverse metal ions such as Co^{2+}, Cu^{2+}, Mn^{2+}, and Zn^{2+} in order to investigate the binding mode and biological importance.[20,25−33] We have also studied the binding of these metal complexes with biological molecules such as albumins and DNA and their potential antioxidant activity. In view of the expanding use of NSAIDs in medicine and the increasing interest in the biological properties of Mn complexes, we have initiated and present herein the synthesis and the characterization of the manganese(II) mixed-ligand complexes of the NSAID tolfenamic acid and nitrogen containing heterocyclic ligands such as pyridine (py), 1,10-phenanthroline (phen), and 2,2′-bipyridylamine (bipyam) and/or the oxygen-donor ligand H_2O and *N*,*N*-dimethylformamide (DMF). The crystal structures of the mononuclear complex $[Mn(tolf\text{-}O)(tolf\text{-}O,O')(phen)(H_2O)]$ (complex **1**), the dinuclear ones $[Mn_2(\mu_2\text{-}H_2O)(\mu_2\text{-}tolf\text{-}O,O')_2(tolf\text{-}O)_2(py)_4]\cdot 1.5MeOH\cdot py$ (complex **2**·1.5MeOH·py) and $[Mn_2(\mu_2\text{-}tolf\text{-}O,O')_2(tolf\text{-}O,O')_2(bipyam)_2]$ (complex **3**), and the 1D polymeric complex $[Mn(\mu_2\text{-}tolf\text{-}O,O')_2(DMF)_2]_n$ (complex **4**) were determined by X-ray structure analysis. The research concerning the antioxidant activity of complexes **1**−**4** has been focused on their ability to scavenge diverse radicals such as 1,1-diphenyl-picrylhydrazyl (DPPH), 2,2′-azinobis(3-ethylbenzothiazoline-6-sulfonic acid) ($ABTS^{+\bullet}$), and hydroxyl ($^{\bullet}OH$) radicals, and to inhibit *in vitro* the soybean lipoxygenase (LOX); the role of NSAIDs and their metal complexes in medicine as anti-inflammatories is often related to their ability to scavenge free radicals. Furthermore, the interaction of complexes **1**−**4** with selected biological macromolecules was investigated with diverse techniques. More specifically, the binding to the albumins which are the proteins responsible for the transport of ions and compounds in the body could differentiate the properties of the drug or reveal novel paths for the drug transportation; therefore, the interaction of compounds **1**−**4** with human (HSA) and bovine serum albumin (BSA) was thoroughly studied with fluorescence spectroscopy. Additionally, the interaction of the complexes with calf-thymus (CT) DNA was studied with UV spectroscopic and DNA-viscosity titrations so as to calculate the binding constants to DNA and to determine the possible mode of binding and with ethidium bromide (EB)-displacement studies from its CT DNA-compound (EB−DNA), performed with fluorescence emission spectroscopy, in order to evaluate the ability to compete with the well-established DNA-intercalator EB, as an indirect means to examine and/or verify the potential intercalation of the complexes to CT DNA.

2. EXPERIMENTAL SECTION

2.1. Materials, Instrumentation, Physical Measurements. Tolfenamic acid, $MnCl_2\cdot 4H_2O$, bipyam, phen, py, KOH, trisodium citrate, NaCl, CT DNA, BSA, HSA, EB, DPPH, ABTS, soybean lipoxygenase, potassium persulfate, EDTA, ascorbic acid, sodium linoleate, NDGA, BHT, trolox, and caffeic acid were purchased from Sigma-Aldrich Co., and all solvents were purchased from Merck. The chemicals and solvents were of reagent grade and were used as purchased.

Infrared (IR) spectra (400−4000 cm^{-1}) were recorded on a Nicolet FT-IR 6700 spectrometer with samples prepared as KBr pellets. UV−visible (UV−vis) spectra were recorded as nujol mulls and in solution at concentrations in the range 10^{-5} to 10^{-3} M on a Hitachi U-2001 dual beam spectrophotometer. C, H, and N elemental analysis were performed on a PerkinElmer 240B elemental analyzer. Molar conductivity measurements were carried out in 1 mM DMSO solution of the complexes with a Crison Basic 30 conductometer. Fluorescence emission spectra were recorded in solution on a Hitachi F-7000 fluorescence spectrophotometer. Viscosity experiments were carried out using an ALPHA L Fungilab rotational viscometer equipped with an 18 mL LCP spindle.

DNA stock solution was prepared by dilution of CT DNA to buffer solution (containing 150 mM NaCl and 15 mM trisodium citrate at pH 7.0) followed by exhaustive stirring at 4 °C for three days, and it was kept at 4 °C for no longer than a week. The concentration of the DNA solution was determined by the measurement of the UV absorption at λ_{max} = 260 nm after 1:20 dilution using ε = 6600 M^{-1} cm^{-1}.[28−30] This CT DNA solution gave the ratio A_{260}/A_{280} (UV absorbance at λ = 260 and 280 nm) in the range of 1.85−1.90, indicating that the DNA was sufficiently free of protein contamination.

2.2.1. Synthesis of $[Mn(tolf)_2(phen)(H_2O)]$, ***1.*** Tolfenamic acid (0.4 mmol, 105 mg) was dissolved in methanol (10 mL) followed by the addition of KOH (0.4 mmol, 22 mg). After 1 h of stirring, the solution was added slowly, and simultaneously with a 10 mL methanolic solution of phen (0.2 mmol, 36 mg), to a methanolic solution (10 mL) of $MnCl_2\cdot 4H_2O$ (0.2 mmol, 40 mg). Yellow crystals of $[Mn(tolf)_2(phen)(H_2O)]$, **1** (95 mg, 60%), suitable for X-ray structure determination, were deposited after three days. Anal. Calcd for $[Mn(tolf)_2(phen)(H_2O)]$ ($C_{40}H_{32}Cl_2MnN_4O_5$) (MW = 774.54): C, 62.03; H, 4.16; N, 7.23. Found: C, 61.83; H, 3.99; N, 6.86. IR (KBr pellet), ν_{max}/cm^{-1} $\nu_{asym}(CO_2)$: 1579 (very strong (vs)). $\nu_{sym}(CO_2)$: 1404, 1372 (strong (s)). $\Delta = \nu_{asym}(CO_2) - \nu_{sym}(CO_2)$: 175, 207 cm^{-1}. UV−vis: λ/nm (ε/M^{-1} cm^{-1}) as nujol mull: 422 (shoulder, (sh)), 299. In DMSO: 425 (sh) (210), 296 (14400). The complex is soluble in DMF and DMSO (Λ_M = 5.0 μS/cm, in 1 mM DMSO solution).

2.2.2. Synthesis of $[Mn_2(tolf)_4(py)_4(H_2O)]\cdot 1.5MeOH\cdot py$, ***2****·1.5MeOH·py.* Complex **2** was prepared by the addition of a methanolic solution (10 mL) of Htolf (0.4 mmol, 105 mg) and KOH (0.4 mmol, 22 mg), which was stirred for 1 h, and a solution of 3 mL pyridine to a methanolic solution (10 mL) of MnCl2·4H_2O (0.2 mmol, 40 mg). Yellowish crystals of $[Mn_2(tolf)_4(py)_4(H_2O)]$, **2** (90 mg, 60%), suitable for X-ray structure determination, were deposited after 30 days. Anal. Calcd for $[Mn_2(tolf)_4(py)_4(H_2O)]\cdot 1.5MeOH\cdot py$ ($C_{82.5}H_{77}Cl_4Mn_2N_9O_{10.5}$) (MW = 1614.21): C, 61.39; H, 4.81; N, 7.81. Found: C, 61.70; H, 4.79; N, 7.42. IR (KBr pellet), ν_{max}/cm^{-1} $\nu_{asym}(CO_2)$: 1584(vs). $\nu_{sym}(CO_2)$: 1386 (vs). Δ = 198 cm^{-1}. UV−vis, λ/nm (ε/M^{-1} cm^{-1}) as nujol mull: 427(sh), 346 (sh), 305. In DMSO: 430 (sh) (260), 350 (sh) (2450), 307 (14 100), 288 (3500). The complex is soluble in CH_3CN, DMF, and DMSO (Λ_M = 6.5 μS/cm, in 1 mM DMSO solution).

2.2.3. Synthesis of $[Mn_2(tolf)_4(bipyam)_2]$, ***3.*** A methanolic solution (10 mL) of KOH (0.4 mmol, 22 mg) and tolfenamic acid (0.4 mmol, 105 mg) was added, after 1 h of stirring, slowly and simultaneously with a methanolic solution (5 mL) of bipyam (0.2 mmol, 34 mg), to a methanolic solution (10 mL) of MnCl2·4H_2O (0.2 mmol, 40 mg). Colorless crystals of $[Mn_2(tolf)_4(bipyam)_2]$, **3** (105 mg, 70%), suitable for X-ray structure determination, were deposited in a couple of days. Anal. Calcd for $[Mn_2(tolf)_4(bipyam)_2]$ ($C_{76}H_{62}Cl_4Mn_2N_{10}O_8$) (MW = 1495.04): C, 61.06; H, 4.18; N, 9.37. Found: C, 61.21; H, 4.29; N, 9.36. IR (KBr pellet), ν_{max}/cm^{-1} $\nu_{asym}(CO_2)$: 1578(vs). $\nu_{sym}(CO_2)$: 1408 (s), 1389 (vs). Δ = 170, 189 cm^{-1}. UV−vis, λ/nm (ε/M^{-1} cm^{-1}) as nujol mull: 418(sh), 349(sh), 311. iI DMSO: 420 (sh) (210), 353(sh) (3700), 314 (17 500). The complex is soluble in DMSO (Λ_M = 4.0 μS/cm, in 1 mM DMSO solution).

2.2.4. Synthesis of $[Mn(tolf)_2(DMF)_2]_n$, ***4.*** A methanolic solution (10 mL) containing tolfenamic acid (0.4 mmol, 105 mg) and KOH (0.4 mmol, 22 mg) was stirred for 1 h. The solution was added dropwise to a methanolic solution (10 mL) of MnCl2·4H_2O (0.2 mmol, 40 mg) followed by the addition of 2 mL of DMF. Pale yellow crystals of $[Mn(tolf)_2(DMF)_2]_n$, **4** (55 mg, 40%), suitable for X-ray structure determination, were collected after four months. Anal. Calcd for $[Mn(tolf)_2(DMF)_2]_n$ ($C_{34}H_{36}Cl_2MnN_4O_6$) (MW = 722.51): C,

dx.doi.org/10.1021/ic4025487 | Inorg. Chem. 2014, 53, 2040−2052

56.52; H, 5.02; N, 7.75. Found: C, 56.39; H, 5.13; N, 8.06. IR (KBr pellet), ν_{max}/cm^{-1} $\nu(C{=}O)_{DMF}$: 1645 (vs). $\nu_{asym}(CO_2)_{tolf}$: 1565 (vs). $\nu_{sym}(CO_2)_{tolf}$: 1395 (vs). Δ = 170, 213 cm^{-1}. UV–vis, λ/nm (ε/M^{-1} cm^{-1}) as nujol mull: 435 (sh), 316, 291. In DMSO: 440 (500), 320 (sh) (5500), 313 (10600), 287 (15 600). The complex is soluble in DMF and DMSO (Λ_M = 8.5 μS/cm, in 1 mM DMSO solution).

2.3. X-Ray Structure Determination. Single-crystal X-ray diffraction data were collected at room temperature (**1**, **2**, **3**) and at 150(2) K (**4**) on an Agilent Technologies SuperNova Dual with an Atlas detector using mirror-monochromatized Mo Kα radiation (λ = 0.71073 Å). The data were processed using CrysAlis Pro.[34] Structures were solved by direct methods[35] implemented in SHELXS-97 and refined by a full-matrix least-squares procedure based on F^2 with SHELXL-97.[36] All the non-hydrogen atoms were refined anisotropically. All the hydrogen atoms were readily located in difference Fourier maps and were subsequently treated as riding atoms in geometrically idealized positions with $U_{iso}(H) = kU_{eq}(C, N)$, where k = 1.5 for NH and methyl groups, which were permitted to rotate but not to tilt, and 1.2 for all other H atoms. Hydrogen atoms attached to water oxygen atoms O(5) in **1** and O(9) in **2** were found in difference Fourier maps and refined fixing the bond lengths and isotropic temperature factors as $U_{iso}(H) = 1.5U_{eq}(O)$. For compound **2**, the crystals were of low quality (R_{int} = 0.0977); however, the data were of sufficient quality to determine the molecular and crystal structure. In the pyridine solvate molecule, the position of the nitrogen atom was not located, and each site was refined as carbon atom (C(77)–C(82)), and the occupancies of hydrogen atoms were set to 5/6. Additionally, one methanol molecule is disordered over two positions in a ratio of 0.57:0.43, and half of a methanol molecule is disordered over the inversion center. The bonds O(11)–C(84) and O(12)–C(85) in methanol molecules were fixed using DFIX instruction. ISOR instruction was used on O(10), O(11), and O(12) atoms of methanol molecules for proper refinement. The hydrogen atoms attached to OH groups were treated as riding atoms in geometrically idealized positions with $U_{iso}(H) = 1.5U_{eq}(O)$. In the final step of the refinement, the hydrogen atoms attached to methanol carbons C(85) and C(84) were set fixed in order to achieve the convergence. Crystallographic data are listed in Table S1, Supporting Information.

2.4. Antioxidant Biological Assays. Each experiment in the *in vitro* assays was performed at least in triplicate, and the standard deviation of absorbance was less than 10% of the mean.

2.4.1. Determination of the Reducing Activity of the Stable Radical DPPH. To an ethanolic solution of DPPH (0.1 mM), an equal volume of ethanolic solution of the tested compounds (0.1 mM) was added. Ethanol was used as a control solution. In order to examine the dependence of the radical scavenging activity from the time of incubation, the absorbance at λ = 517 nm was recorded at room temperature after 20 and 60 min.[28,37] The ability of the tested compounds to scavenge DPPH radicals was expressed as the percentage reduction of the absorbance of the initial DPPH solution (RA%). NDGA and BHT were used as reference compounds.

2.4.2. Competition of the Tested Compounds with DMSO for Hydroxyl Radicals. The hydroxyl radicals as generated by the Fe^{3+}/ascorbic acid system were detected by the determination of formaldehyde produced from the oxidation of DMSO according to Kontogiorgis et al.[28,37] The reaction mixture contained EDTA (0.1 mM), Fe^{3+} (167 μM), DMSO (33 mM) in phosphate buffer (50 mM, pH 7.4), the tested compounds (0.1 mM), and ascorbic acid (10 mM). The reaction was stopped with CCl_3COOH (17% w/v) after 30 min of incubation (37 °C), and the absorbance at λ = 412 nm was measured. The competition of the compounds with DMSO for $^{\bullet}OH$, generated by the Fe^{3+}/ascorbic acid system was expressed as the percent inhibition of formaldehyde production and was used in order to evaluate the ability of the tested compounds to scavenge hydroxyl radicals ($^{\bullet}OH$%). Trolox was used as a reference compound.

2.4.3. Assay of Radical Cation Scavenging Activity. $ABTS^{\bullet+}$ was produced by reacting an aqueous ABTS stock solution (2 mM) with 0.17 mM potassium persulfate. The mixture was allowed to stand in the dark at room temperature for 12–16 h before use.[28,37] ABTS and potassium persulfate react stoichiometrically at a ratio of 1:0.5; therefore, the oxidation of the ABTS was incomplete. The oxidation of the ABTS started immediately, but the absorbance of the solution became maximal and stable after 6 h. In this form, the radical is stable for more than two days, if stored in the dark at room temperature. The solution of $ABTS^{\bullet+}$ was diluted with ethanol so as to give an absorption of 0.70 at 734 nm. Afterward, 10 μL of diluted tested compounds or the reference compound trolox in DMSO (0.1 mM) were added, and the absorbance was measured 1 min after the initial mixing.[38,39] The ability of the tested compounds to scavenge ABTS radicals was expressed as the percentage inhibition of the absorbance of the initial ABTS solution (ABTS%).

2.4.4. Soybean Lipoxygenase Inhibition Study in Vitro. The soybean lipoxygenase inhibition was evaluated *in vitro* as reported in the literature.[37] The tested compounds were dissolved in ethanol and were incubated at room temperature with sodium linoleate (0.1 mM) and 0.2 mL of enzyme solution ($1/9 \times 10^{-4}$ w/v in saline). The conversion of sodium linoleate to 13-hydroperoxylinoleic acid was studied by the absorbance at λ = 234 nm and compared with the appropriate standard inhibitor caffeic acid.

2.5. Albumin Binding Studies. Albumin binding studies have been performed via tryptophan fluorescence emission quenching experiments using BSA (3 μM) or HSA (3 μM) in a buffer solution (15 mM trisodium citrate, 150 mM NaCl, pH 7.0). The quenching of the fluorescence emission intensity of BSA or HSA tryptophan residues was measured at $\lambda_{em,max}$ = 343 or 351 nm, respectively, and was monitored using tested compounds **1**–**4** as quenchers with increasing concentration.[28−30] Fluorescence emission spectra were recorded in the range 300–500 nm with $\lambda_{exc,max}$ = 295 nm. The fluorescence emission spectra of tested compounds **1**–**4** were recorded under the same experimental conditions and exhibited a maximum emission at 330 nm.[28,29] Therefore, the quantitative studies of the serum albumin fluorescence emission spectra were performed after their correction by subtracting the corresponding fluorescence emission spectra of the quenchers. The Stern–Volmer (eq S1) and Scatchard equations (eq S2) and corresponding graphs were used for the study of the interaction of the tested compounds with serum albumins.

2.6. DNA-Binding Studies. The binding of complexes **1**–**4** with CT DNA was studied by UV spectroscopy as a means to investigate the possible DNA-binding modes and to determine the DNA-binding constants (K_b). In UV titration experiments, the UV spectra of a CT DNA solution (0.15–0.20 mM) were recorded in the presence of each tested compound at increasing [compound]/[CT DNA] mixing ratios (r). The DNA-binding constants, K_b, of the complexes **1**–**4** with CT DNA were determined using the UV spectra of a DMSO solution of the tested compound (10^{-5} M) in the presence of DNA for diverse r values. Furthermore, no changes in the spectra of the DNA solution were observed during control experiments with DMSO.

The measurements of the viscosity of a DNA solution (0.1 mM) in the presence of increasing amounts of tested compounds **1**–**4** were performed with an ALPHA L Fungilab rotational viscometer at 100 rpm, which is equipped with an 18 mL LCP spindle. The obtained data were given as $(\eta/\eta_0)^{1/3}$ versus r, where η_0 and η are the viscosity of DNA solution in the absence and presence of the tested compound, respectively.

The EB-competitive studies of each tested compound were carried out with fluorescence emission spectroscopy so as to examine whether the tested compounds **1**–**4** can displace EB from its CT DNA-EB complex, which was initially prepared by the addition of 20 μM EB and 26 μM CT DNA in buffer solution (150 mM NaCl, 15 mM trisodium citrate, pH 7.0). The DNA-intercalating effect of complexes **1**–**4** was studied by their stepwise addition into a solution of the EB–DNA complex. The influence of such additions was studied by recording the variation of fluorescence emission spectra.

3. RESULTS AND DISCUSSION

3.1. Synthesis of the Complexes. The synthesis of the complexes has been achieved in methanol via the aerobic reaction of tolfenamic acid, previously deprotonated by KOH,

dx.doi.org/10.1021/ic4025487 | Inorg. Chem. 2014, 53, 2040–2052

with $MnCl_2·4H_2O$ and the corresponding *N*,*N*′-donor ligand (phen, py or bipyam) or O−donor (DMF). The resultant complexes **1**−**4** are soluble mainly in DMSO and most of them in DMF and are nonelectrolytes ($\Lambda_M \leq 9$ μS/cm, in 1 mM DMSO solution). The novel manganese complexes were characterized by physicochemical (elemental analysis and variable-temperature magnetic measurements) and spectroscopic (IR and UV−vis spectroscopy) techniques in the solid state and by UV−vis spectroscopy in solution. The crystal structures of complexes **1**−**4** were determined via X-ray crystallography.

3.2. Spectroscopic Study of the Complexes. The deprotonation and the binding mode of tolfenamic acid were examined by IR spectroscopy. The deprotonation of Htolf was confirmed by the disappearance in IR spectra of the complexes of the band observed in the IR spectrum of Htolf at 3355 (br,m) cm^{-1}, which is attributed to the ν(O−H) stretching vibration. Furthermore, the absorption bands at 1661(s) cm^{-1} and 1265(s) cm^{-1} observed for Htolf and attributed to the $\nu(C{=}O)_{carb}$ and $\nu(C{-}O)_{carb}$ stretching vibrations of the carboxylic moiety (−COOH), respectively, shifted in the IR spectra of the complexes, in the range 1565−1584 cm^{-1} and 1372−1408 cm^{-1} assigned to antisymmetric, $\nu_{asym}(C{=}O)$, and symmetric, $\nu_{sym}(C{=}O)$, stretching vibrations of the carboxylate group, respectively. The values of the parameter Δ [= $\nu_{asym}(C{=}O) - \nu_{sym}(C{=}O)$], a tool indicative of the binding mode of carboxylate ligands, fall in the range 170−207 cm^{-1}, suggesting an asymmetrical binding mode of the tolfenamato ligand.[25,26]

The UV−vis spectra of the complexes recorded in solution (DMSO) and in nujol (as a mull) are similar, showing that the compounds have the same structure in solution. The band at 420−400 nm (ε = 210−500 M^{-1} cm^{-1}) can be attributed to a charge transfer transition while the bands found in the UV region are assigned to intraligand transitions of the complexes. The integrity of the compounds in solution may be concluded because of the same UV−vis spectral features presented in the solid state (nujol), in solution (DMSO), and in the presence of the buffer solution used in the biological experiments (150 mM NaCl, 15 mM trisodium citrate, pH = 7.0) and the molar conductivity measurements, which suggest nondissociation.[6,31]

3.3. Structure of the Complexes. *3.3.1. Crystal Structure of [Mn(tolf-O)(tolf-O,O′)(phen)(H_2O)],* ***1****.* The molecular structure of [Mn(tolf-O)(tolf-O,O′)(phen)(H_2O)] is depicted in Figure 1, and selected bond distances and angles are cited in Table S2. Complex **1** is mononuclear, and the two tolfenamato ligands are deprotonated and behave in different binding modes: one tolfenamato ligand is monodentately coordinated to the manganese ion via a carboxylate oxygen atom (O(3)), while the other tolfenamato ligand is bound in an asymmetric bidentate chelating mode (C(1)−O(1) = 1.272(2) Å and C(1)−O(2) = 1.265(2) Å). The structure is further stabilized by intramolecular H bonds formed by the uncoordinated O(4) and the coordinated aqua ligand (via H(1)) and the coordinated O(2) and O(3) atoms and the NH group of the tolfenamato ligands (Table S3). Intermolecular H bonds are formed via H(2) of the coordinated aqua ligand and O(1)′ of a neighboring molecule (Figure S1).

This binding mode albeit not unprecedented is rare. Eight crystal structures of manganese(II) complexes bearing a phenanthroline (or derivative), an aqua ligand, and two carboxylate ligands coordinated to Mn according to the aforementioned mode have been found in the CCDC database;

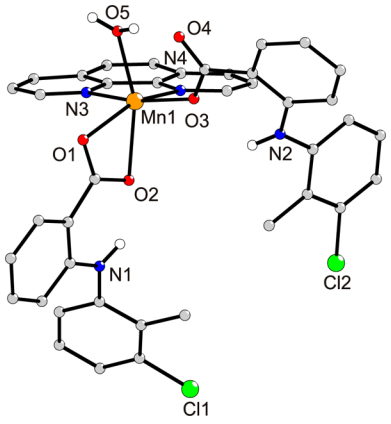

Figure 1. The molecular structure and partial labeling of **1** with only the heteroatoms labeled. Selected bond distances: Mn(1)−O(1) = 2.2120(14) Å, Mn(1)−O(2) = 2.2646(14) Å, Mn(1)−O(3) = 2.1009(16) Å, Mn(1)−O(5) = 2.1519(17) Å, Mn(1)−N(3) = 2.273(2) Å, Mn(1)−N(4) = 2.2608(18) Å; Selected bond angles: O(1)−Mn(1)−N(4) = 153.49(6)°, O(2)−Mn(1)−O(5) = 156.82(6)°, O(3)−Mn(1)−N(3) = 163.07(6)°.

nevertheless, it is rare in regard to mononuclear Mn(II) complexes since only three compounds are known (with indole-2-carboxylate,[40] *p*-methoxy-benzoate,[41] and p-hydroxy-benzoate[42]), while the others are di- or tetra-nuclear complexes.

The manganese atom is six-coordinate with a distorted octahedral environment formed by two nitrogen atoms from the phen ligand, three oxygen atoms provided by the two tolfenamato ligands, and an aqua oxygen atom. The bond distances around the manganese atom are not equal, with the monodentate coordinated carboxylate oxygen atom O(3) (Mn(1)−O(3) = 2.1009(16) Å) and the aqua oxygen O(5) (Mn(1)−O(5) = 2.1519(17) Å) being closer to Mn than the chelating carboxylate oxygen atoms O(1) and O(2) (Mn(1)−O(1) = 2.2120(14) Å and Mn(1)−O(2) = 2.2646(14) Å) and the phen nitrogen atoms N(3) and N(4) (Mn(1)−N(3) = 2.273(2) Å and Mn(1)−N(4) = 2.2608(18) Å). The uncoordinated oxygen atom O(4) lies at 3.368 Å away from the manganese atom. The N(3)−Mn(1)−N(4) angle observed is 73.14(7)° and is similar to reported values of other chelating polycyclic diimines.[26−30] The phen ligand is almost planar with the manganese atom lying ∼0.134 Å out of this plane.

Supramolecular aggregation of **1** is stabilized by $\pi-\pi$ interactions with *Cg*4···*Cg*4^{ii} and *Cg*6···*Cg*7^{iii} centroid-to-centroid distances 3.5182(16) and 3.9212(14) Å, respectively [*Cg*4, *Cg*6, and *Cg*7 are N(4)/C(37)/C(36)/C(38)−C(40), C(8)−C(13), and C(16)−C(21) ring centroids, respectively; symmetry codes: (ii) 1 − *x*, 1 − *y*, 1 − *z*; (iii) −1 + *x*, *y*, *z*; (iv) 1 + *x*, *y*, *z*] (Figure S2) and by a network of weak C−H···*Cg*(arene), C−Cl···*Cg*(arene), and C═O···*Cg*(arene) interactions.

3.3.2. Crystal Structure of [Mn_2(μ_2-H_2O)(μ_2-tolf-O,O′)$_2$(tolf-O)$_2$(py)$_4$]·1.5MeOH·py, ***2****·1.5MeOH·py.* The molecular structure of [Mn_2(μ_2-H_2O)(μ_2-tolf-O,O′)$_2$(tolf-O)$_2$(py)$_4$] is shown in Figure 2, and selected bond distances and angles are given in Table S4. It is a dinuclear complex with four deprotonated tolfenamato ligands being in two different binding modes; two tolfenamato ligands are bidentately coordinated to manganese ion via two carboxylate oxygen atoms (O(1) and O(2), O(3) and O(4)) forming two syn-syn O,O′-carboxylate bridges between Mn(1) and Mn(2), while the other two tolfenamato ligands are bound to a manganese ion in a monodentate

dx.doi.org/10.1021/ic4025487 | *Inorg. Chem.* 2014, 53, 2040−2052

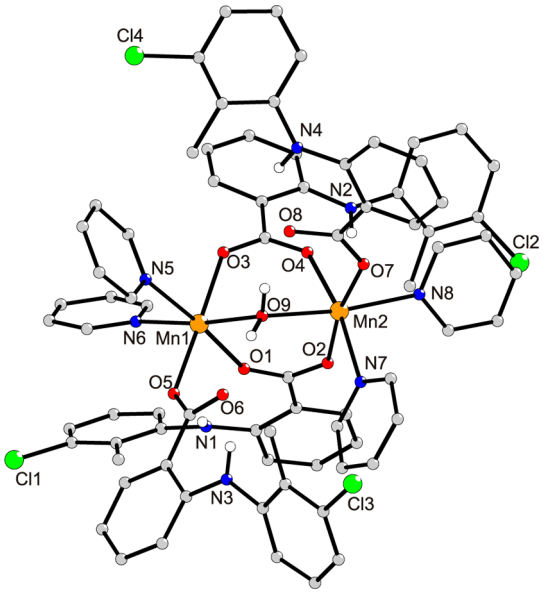

Figure 2. The molecular structure and partial labeling of **2** with only the heteroatoms labeled. Selected bond distances: Mn(1)−O(1) = 2.176(3) Å, Mn(1)−O(3) = 2.122(3) Å, Mn(1)−O(5) = 2.147(3) Å, Mn(1)−O(9) = 2.218(3) Å, Mn(1)−N(5) = 2.326(4) Å, Mn(1)−N(6) = 2.294(4) Å, Mn(2)−O(2) = 2.122(3) Å, Mn(2)−O(4) = 2.149(3) Å, Mn(2)−O(7) = 2.126(3) Å, Mn(2)−O(9) = 2.298(3) Å, Mn(2)−N(7) = 2.325(4) Å, Mn(2)−N(8) = 2.282(3) Å, Mn(1)···Mn(2) = 3.709 Å. Selected bond angles: O(1)−Mn(1)−N(5) = 175.42(13)°, O(3)−Mn(1)−O(5) = 176.36(12)°, O(9)−Mn(1)−N(6) = 173.10(11)°, O(2)−Mn(2)−O(7) = 169.96(11)°, O(4)−Mn(2)−N(7) = 170.05(13)°, O(9)−Mn(2)−N(8) = 169.51(12)°, Mn(1)−O(9)−Mn(2) = 110.42(12)°.

binding mode. The aqua ligand is bridging the two manganese atoms bound via its oxygen atom O(9). Each manganese atom is six-coordinate with a N_2O_4 coordination sphere, and its environment is described as a distorted octahedron, the vertices of which are occupied by three tolfenamato oxygen atoms, an aqua oxygen, and two pyridine nitrogen atoms from the bound pyridine ligands.

All possible bridging arrangements of the $[Mn_2(\mu\text{-}H_2O)(\mu\text{-carboxylato})_2]$ moiety are shown in Scheme 2A, with an aqua bridge and (I) two O,O′-carboxylate bridges, (II) a O,O′- and a O,O-carboxylate bridge, or (III) two O,O-carboxylate bridges. Almost half of the approximately 35 crystal structures found in the CCDC database adopting motif I are of dinuclear complexes; the other complexes present mainly a polymeric structure. The determined crystal structure of complex **2** presents the arrangement motif I with the Mn(1)···Mn(2) = 3.709 Å being in the Mn···Mn distance range found in such complexes (3.484−3.777 Å).[43−47] No dinuclear complexes bearing motifs II or III were found in the literature, but crystal structures of tri-, tetra-, hexa-, and octa-nuclear and polymeric complexes containing such motifs have been reported. The $Mn-O_{aqua}-Mn$ angle [Mn(1)−O(9)−Mn(2) = 110.42(12)°] is within the range of the values reported (101.94−114.97°) for dinuclear complexes $[Mn_2(\mu\text{-}H_2O)(\mu\text{-carboxylato})_2]$ bearing arrangement motif I.[43−47]

The bond distances around the manganese atoms are not equal, with the $Mn-O_{carboxylate}$ bond distances being shorter (2.122(3)−2.176(3) Å) than $Mn-O_{aqua}$ (2.218(3)−2.298(3) Å) and $Mn-N_{pyridine}$ bond distances being the longest (2.282(3)−2.326(4) Å). The uncoordinated oxygens atoms O(6) and O(8) are at 3.374 and 3.353 Å away from the manganese atoms, Mn(1) and Mn(2), respectively.

The dinuclear structure is further stabilized by intramolecular H bonds formed by the uncoordinated tolfenamato oxygens atoms O(6) and O(8) to the coordinated aqua ligand (via H(1) and H(2)) and the NH groups of the tolfenamato ligands as well as of the coordinated oxygen atoms O(1) and O(4) to the NH groups of the corresponding tolfenamato ligands (Table S3, Figure S3) and also by intramolecular $\pi-\pi$ interactions with *Cg*4···*Cg*8 and *Cg*6···*Cg*10 centroid-to-centroid distances 3.789(3) and 4.153(3) Å, respectively [*Cg*4, *Cg*6, *Cg*8, and *Cg*10 are N(6)/C(62)−C(66), N(8)/C(72)−C(76), C(22)−C(27), and C(50)−C(55) ring centroids, respectively]. Two neighboring complexes are connected via intermolecular $\pi-\pi$ interactions with a *Cg*10···*Cg*14^{i} centroid-to-centroid distance (3.975(4) Å), symmetry code: (i) $2-x, -y, 2-z$ (Figure S4). The structure is further stabilized by weak interactions of the type C−H···*Cg*(arene) and C−Cl···*Cg*(arene).

Scheme 2. Arrangement Motifs of the (A) $[Mn_2(\mu\text{-}H_2O)(\mu\text{-RCOO})_2]$ and (B) $[Mn_2(\mu\text{-RCOO})_2]$ Moiety

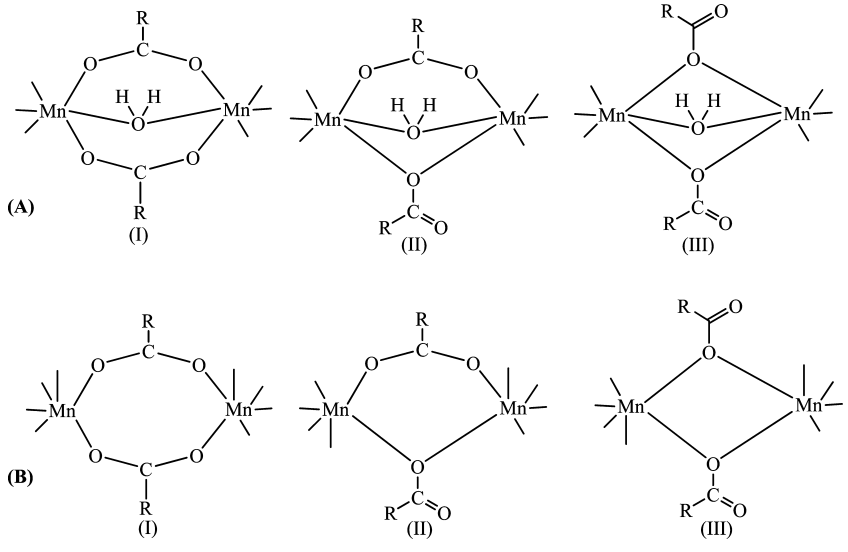

dx.doi.org/10.1021/ic4025487 | Inorg. Chem. 2014, 53, 2040−2052

*3.3.3. Crystal Structure of [$Mn_2(\mu_2$-tolf-O,O′)$_2$(tolf-O,O′)$_2$(bipyam)$_2$], **3**.* The molecular structure of [$Mn_2(\mu_2$-tolf-O,O′)$_2$(tolf-O,O′)$_2$(bipyam)$_2$] is given in Figure 3, and selected bond distances and angles are cited in Table S5. The crystal structure of **3** is composed of centrosymmetric dimers. Two bidentate tolfenamato ligands form syn−anti bridges between isolated pairs of manganese atoms separated by 4.548 Å. The other two tolfenamato ligands and two bipyam ligands are bound to the Mn(II) atoms in a bidentate chelating mode. The bridging tolfenamato ligands are bound to two Mn(II) metal ions in a symmetric fashion [Mn(1)−O(3) = 2.1023(19) Å, Mn(1)−O(4) = 2.087(2) Å], while the bidentate chelating tolfenamato ligands are bound to a Mn(II) ion in an asymmetric mode [Mn(1)−O(1) = 2.2152(19) Å and Mn(1)−O(2) = 2.3632(19) Å]. Each manganese atom is six-coordinate with the two nitrogen atoms N(3) and N(4) (Mn(1)−N(3) = 2.266(2) Å and Mn(1)−N(4) = 2.245(2) Å) of the bipyam molecule occupying the remaining two positions. Thus, the polyhedron can be described as having a distorted octahedral geometry. The N(3)−Mn(1)−N(4) angle observed (= 80.63(8)°) lies in the range of expected values of complexes with chelating bipyam ligands.[32,48]

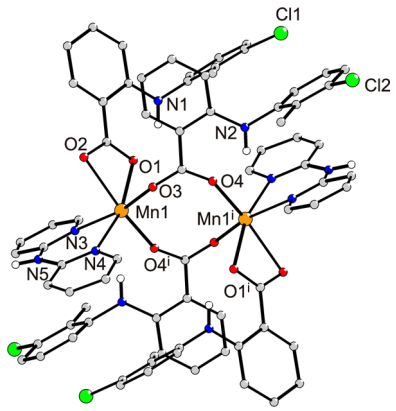

Figure 3. The molecular structure and partial labeling of **3** with only the heteroatoms labeled. Selected bond distances: Mn(1)−O(1) = 2.2152(19) Å, Mn(1)−O(2) = 2.3632(19) Å, Mn(1)−O(3) = 2.1023(19) Å, Mn(1)−O(4)′ = 2.087(2) Å, Mn(1)−N(3) = 2.266(2) Å, Mn(1)−N(4) = 2.245(2) Å, Mn1···Mn1# = 4.548 Å. Selected bond angles: O(1)−Mn(1)−N(4) = 163.53(8)°, O(2)−Mn(1)−O(4)′ = 152.03(9)°, O(3)−Mn(1)−N(3) = 164.50(8)°.

The present bridging mode, i.e., two O,O′-carboxylate bridges (Scheme 2B.I), is one of the three possible combinations I−III for the [$Mn_2(\mu$-RCOO)$_2$] moiety, which are found in polynuclear Mn(II) complexes. In the case of dinuclear Mn(II) complexes, the arrangement motifs I and III have been reported (Scheme 2B). The Mn···Mn separation distance found in the crystal structure of **3** (4.548 Å) lies within the distance range in Mn(II) complexes with motif I (4.1−4.874 Å),[49−51] while in the complexes of motif III, this distance varies from 3.334 Å to 3.726(4) Å.[50−54]

The structure is further stabilized by intermolecular H bonds formed by the coordinated tolfenamato oxygen atoms O(2) to the NH groups of the bipyam ligands of a neighboring molecule and by intramolecular H bonds formed by the coordinated tolfenamato oxygens atoms O(1) and O(4) to the NH groups of the corresponding tolfenamato ligands (Table S3, Figure S5). The crystal structure of **3** is further stabilized by $\pi-\pi$ interactions with *Cg*3···*Cg*4^{ii} and *Cg*3···*Cg*8 centroid-to-centroid distances 4.115(2) and 3.800(2) Å, respectively [*Cg*3, *Cg*4, and *Cg*8 are N(3)/C(29)−C(33), N(4)/C(34)−C(38), and C(22)−C(27) ring centroids, respectively; symmetry code: (ii) 1 − *x*, 1 − *y*, −*z*] (Figure S6), and by weak C−H··· *Cg*(arene) interactions.

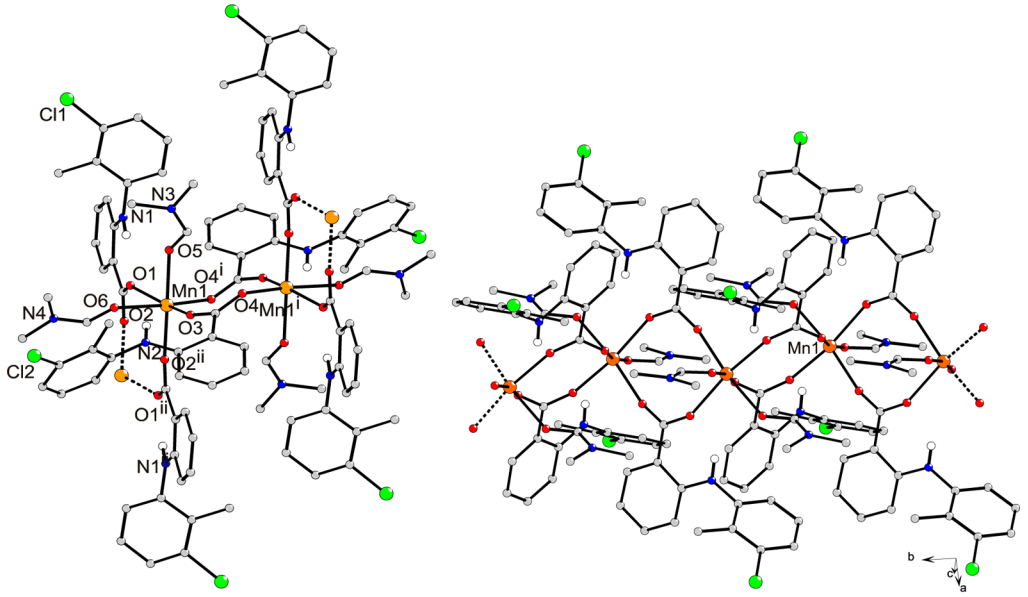

(A) **(B)**

Figure 4. (A) The molecular structure and partial labeling of **4** with only the heteroatoms labeled. Selected bond distances: Mn(1)−O(1) = 2.1395(13) Å, Mn(1)−O(2)′ = 2.0924(13) Å, Mn(1)−O(3) = 2.1354(13) Å, Mn(1)−O(4)′ = 2.1376(13) Å, Mn(1)−O(5) = 2.1935(13) Å, Mn(1)−O(6) = 2.2555(14) Å, Mn(1)...Mn(1)′ = 4.586, 4.614 Å. Selected bond angles: O(1)−Mn(1)−O(3) = 159.69(5)°, O(2)−Mn(1)−O(5) = 169.37(6)°, O(4)′−Mn(1)−O(6) = 170.60(5)°. (B) The polymeric structure of complex **4** (orange for Mn, red for O, blue for N, green for Cl, gray for C, and white for H atoms).

dx.doi.org/10.1021/ic4025487 | *Inorg. Chem.* 2014, 53, 2040−2052

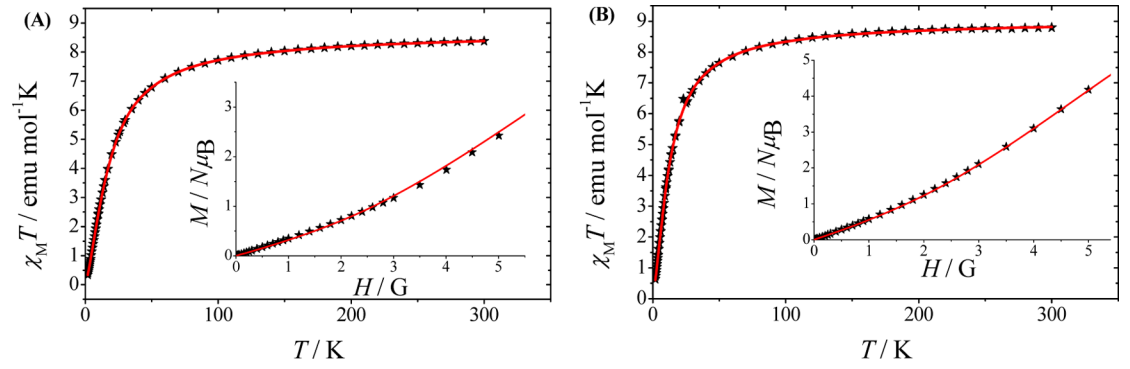

Figure 5. Temperature dependence of $\chi_M T$ (χ_M being the magnetic susceptibility for two Mn^{II} ions) for complexes (A) **2** and (B) **3**. The solid line represents the best fit according to the model discussed in the text. Insets: Magnetization curve at 2 K in the field range 0−5 T.

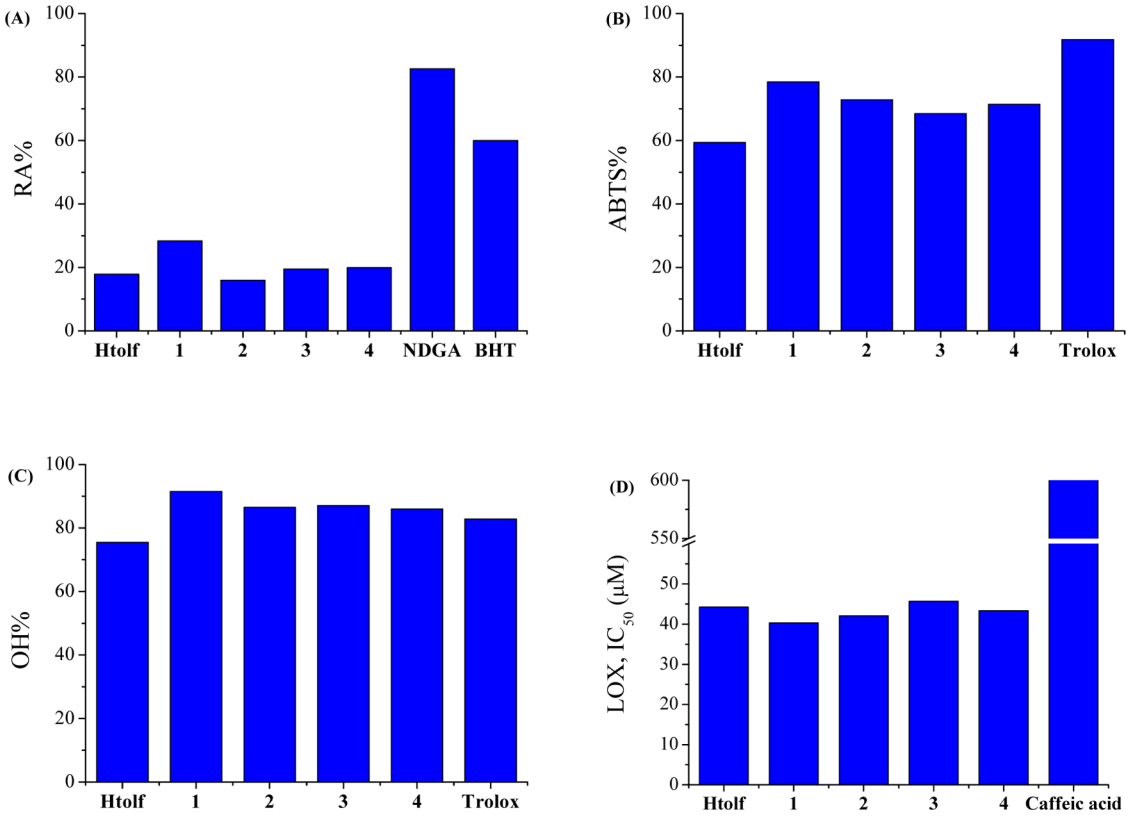

Figure 6. (A) % DPPH scavenging ability (RA%), (B) % superoxide radical scavenging activity (ABTS%), (C) competition % with DMSO for hydroxyl radical ($^{\bullet}$OH%), and (D) *in vitro* inhibition of soybean lipoxygenase (LOX) (IC_{50}, in μM) for Htolf, its complexes **1**−**4**, and reference compounds.

3.3.4. Crystal Structure of [Mn(μ_2-tolf-O,O′)$_2$(DMF)$_2$]$_n$, 4. The molecular structure of $[Mn(tolf)_2(DMF)_2]_n$ is depicted in Figure 4A, and selected bond distances and angles are given in Table S6. The zigzag polymeric structure of the compound is infinitely extended along two (*a* and *b*) crystallographic directions. The octahedral Mn^{2+} centers are bridged by two O,O′-carboxylate groups that form this infinite chain. The centrosymmetric coordination sphere around Mn consists of two oxygen atoms from DMF ligands and four oxygens from the tolfenamato ligands. The tolfenamato ligands are bidentate forming syn−syn bridges between two Mn atoms; such a bridging arrangement generates the one-dimensional polymeric structure (Figure 4B) in which the closest Mn···Mn separation is 4.600(14) Å, lying in the range (4.065−4.823 Å) found for polymeric Mn(II) complexes bridged by two O,O′-carboxylate groups.[55−58]

The $Mn-O_{carboxylate}$ distances [Mn(1)−O(1) = 2.1395(13) Å, Mn(1)−O(2)′ = 2.0924(13) Å, Mn(1)−O(3) = 2.1354(13) Å, and Mn(1)−O(4)′ = 2.1376(13) Å] are similar and shorter than the $Mn-O_{DMF}$ distances [Mn(1)−O(5) = 2.1935(13) Å and Mn(1)−O(6) = 2.2555(14) Å]. The structure is further stabilized by intramolecular H bonds formed by the coordinated tolfenamato oxygen atoms O(1) and O(3) to the NH groups of the corresponding tolfenamato ligands (Table S3). The crystal structure is also stabilized by weak C−H··· *Cg*(arene) interactions; however, there are no significant $\pi-\pi$ interactions present.

3.4. Magnetic Properties of Complexes 2 and 3. The temperature dependence of $\chi_M T$ (χ_M being the magnetic

dx.doi.org/10.1021/ic4025487 | *Inorg. Chem.* 2014, 53, 2040−2052

susceptibility for two Mn^{II} ions) for complexes **2** and **3** is shown in Figure 5.[59] The $\chi_M T$ value is 8.4/8.8 emu mol^{-1} K at 300 K (close to the value expected for two isolated Mn(II) ions), and until 50 K there is a smooth decrease, while after that temperature and until 2 K a more pronounced one occurs, reaching the value of 0.4/0.6 emu mol^{-1} K at 1.8 K. The shape of these susceptibility curves is characteristic of the occurrence of weak antiferromagnetic interactions between the Mn(II) centers. A fitting procedure was carried out using the simple Hamiltonian model for two interacting spins ($H = -2JS_1 \cdot S_2$), and the fitted results are shown in the same figures as solid lines. The obtained values are $J = -1.3/-0.9$ cm^{-1} and $g = 1.99/2.03$, denoting very weak antiferromagnetic interactions between the two ions, and are lying in the range of J values found in the literature.[43−47,49−55]

In the insets of Figure 5, the isothermal magnetization curves at $T = 2$ K in the applied field 0−5 T are shown. The same magnetic model was used to simulate the magnetization data using the values obtained from the fitting procedure of the susceptibility data, and the results are shown as solid lines in the same figures, confirming the correctness of the model. It must be pointed out that in both cases there is a clear contribution of excited states to the $S = 0$ ground state in view of the fact that the magnetization curve exhibits a linear increase at high magnetic fields with no saturation values.

3.5. Biological Assays. *3.5.1. Antioxidant Capacity.* Free radicals are compounds having an important role in the inflammatory process. NSAIDs can also act either as inhibitors of free radical production or as radical scavengers;[60] thus, the antioxidant activity of the NSAIDs and their metal complexes could be related to tentative anti-inflammatory and anticancer activity. Novel potentially effective drugs may originate from compounds bearing antioxidant properties with a role in the treatment of inflammation. Furthermore, the role of Mn superoxide dismutase (MnSOD), which is one of the most important manganese enzymes, is the protection of the organisms from potentially damaging oxygen radicals by catalyzing the disproportionation of superoxide to oxygen and hydrogen peroxide.[1,61] The ability of complexes **1**−**4** to scavenge DPPH, ABTS, and hydroxyl radicals and their *in vitro* soybean lipoxygenase inhibition has been evaluated and compared to that of widely used and well-known antioxidant agents (e.g., butylated hydroxytoluene (BHT), 6-hydroxy-2,5,7,8-tetramethylchromane-2-carboxylic acid (trolox), nordihydroguaiaretic acid (NDGA), and caffeic acid) used as reference compounds in order to estimate a potential antioxidant ability.

The ability of the compounds to scavenge DPPH radicals is usually related to anti-inflammatory and antiaging activity.[37] Compounds able to scavenge DPPH radicals are interesting and can provide protection against inflammation and rheumatoid arthritis, leading to potentially effective drugs. 1,1-Diphenyl-picrylhydrazyl is a stable free radical and exhibits a strong absorption band at $\lambda_{max} = 517$ nm, which, upon donation of protons from antioxidants, decreases. The measurements were performed after 20 and 60 min, and there were not any significant changes, proving that the scavenging activity of complexes is not time-dependent (Table S7). The ability of the complexes to scavenge DPPH radicals is low to moderate in comparison to NDGA and BHT (reference compounds) and similar or higher than free Htolf, with **1** being the most active DPPH scavenger among complexes **1**−**4** (Figure 6A).

The ability of the compounds to scavenge cationic ABTS radicals ($ABTS^{+\bullet}$) is related to the total antioxidant activity of the compounds and its magnitude.[29] The complexes show significantly higher ABTS radical scavenging activity than free Htolf but lower than the reference compound trolox, with complex **1** exhibiting the highest ability to scavenge ABTS (ABTS% = 78.44 (±0.38)%) among the complexes (Table S7). The complexes are more active ABTS scavengers than free Htolf (Figure 6B) in agreement with the DPPH scavenging studies.

The study of the hydroxyl scavenging activity of the tested compounds is important since hydroxyl radicals are among the most reactive oxygen species. Compounds capable of scavenging hydroxyl radicals serve also as protectors via the activation of the synthesis of the prostaglandins. It is known that the superoxide anion radicals are generated by phagocytes at the inflamed site during the inflammatory process and are connected to other oxidizing species such as $^{\bullet}OH$.[29] All complexes (Table S7) exhibit higher competition with DMSO (33 mM) at 0.1 mM for hydroxyl free radicals than free tolfenamic acid and the reference compound trolox with complex **1** (Figure 6C) being the most active compound ($^{\bullet}OH$ % = 91.47 (±0.51) %).

Lipoxygenases (LOXs) are enzymes playing a significant role in the pathophysiology of several allergic and inflammatory diseases because LOXs are involved in the transformation of arachidonic acid to leukotrienes. The products derived from the oxygenation catalyzed by LOX are responsible for the development of asthmatic responses, psoriasis, and rheumatoid arthritis.[62] From this point of view, most of the compounds that inhibit LOX activity are excellent antioxidants or free radical scavengers.[63] LOXs are dioxygenases containing a nonheme high-spin iron in the enzyme active site per molecule, which is at a +3 oxidation state when activated and at +2 when in the inactive state. Therefore, a relationship of the LOX inhibitors between their ability to inhibit LOX and to reduce the Fe(III) at the active site to the catalytically inactive Fe(II) has been widely reported; most LOX inhibitors are ideal Fe(III) ligands.[64] As another marker of the antioxidant activity, the *in vitro* inhibition of the compounds against soybean LOX was evaluated. All complexes exhibit noteworthy inhibitory activity against soybean lipoxygenase (Table S7), especially when compared to caffeic acid (IC_{50} = 600 μM), which is the reference compound. The complexes present slightly better LOX inhibition activity than free Htolf, and **1** (Figure 6D) is the most active LOX inhibitor (IC_{50} = 40.31 (±0.72) μM).

In conclusion, the complexes exhibit similar or higher radical scavenging and LOX inhibitory activity than free tolfenamic acid, and complex **1** can be considered the most active scavenger among the complexes examined. This is in agreement with the reports for a series of Co(II), Ni(II), Cu(II), Zn(II), and Pd(II) complexes exhibiting enhanced antioxidant activity compared to corresponding free ligands.[29,32,48,65−67] Additionally, complexes active against DPPH radicals[68,69] and others exhibiting hydroxyl and ABTS[29,32,48,65−68,70] scavenging activity have been reported. Mn(II)−tolfenamato complexes **1**−**4** exhibit low to moderate activity against DPPH and high activity against hydroxyl and ABTS radicals, a fact that could be considered as first evidence of selective scavenging activity of the complexes against hydroxyl and ABTS radicals.

3.5.2. Interaction of the Compounds with Serum Albumins. Serum albumin (SA) is among the most abundant proteins in plasma. Its mission is to carry ions and drugs

dx.doi.org/10.1021/ic4025487 | Inorg. Chem. 2014, 53, 2040−2052

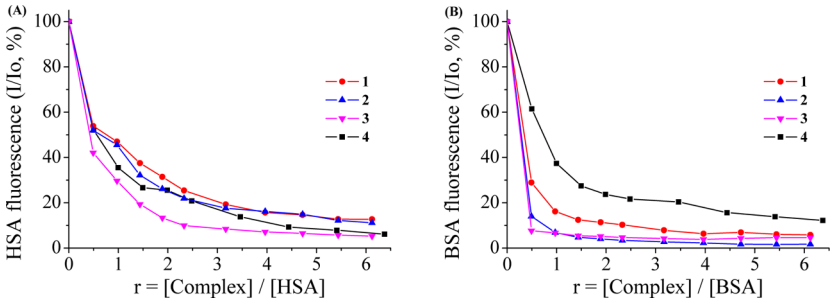

Figure 7. (A) Plot of % relative HSA fluorescence emission intensity (I/Io%) at $\lambda_{em,max}$ = 351 nm of a buffer solution (150 mM NaCl, 15 mM trisodium citrate, pH = 7.0) of HSA (3 μM) in the presence of compounds **1**−**4** at diverse *r* values (= [complex]/[HSA]) vs *r* (12.5% of the initial HSA fluorescence intensity for **1**, 11% for **2**, 5% for **3**, and 6% for **4**). (B) Plot of % relative BSA fluorescence emission intensity (I/Io%) at $\lambda_{em,max}$ = 343 nm of a buffer solution (150 mM NaCl, 15 mM trisodium citrate, pH = 7.0) of BSA (3 μM) in the presence of complexes **1**−**4** at diverse *r* values (= [complex]/[BSA]) vs *r* (6% of the initial BSA fluorescence intensity for **1**, 2% for **2**, 4.5% for **3**, and 12% for **4**).

Table 1. The SA Constants and Parameters (K_{sv}, k_q, K, n) for Htolf and Its Complexes 1−4

BSA				
compound	K_{sv} (M^{-1})	k_q (M^{-1} s^{-1})	K (M^{-1})	n
Htolf[25]	2.18 (±0.12) × 10^5	2.18 (±0.12) × 10^{13}	1.60 (±0.14) × 10^5	1.11
$[Mn(tolf)_2(phen)(H_2O)]$, **1**	7.62 (±0.55) × 10^5	7.62 (±0.55) × 10^{13}	1.86 (±0.09) × 10^6	0.98
$[Mn_2(tolf)_4(py)_4(H_2O)]$, **2**	3.24 (±0.17) × 10^6	3.24 (±0.17) × 10^{14}	4.32 (±0.14) × 10^6	0.99
$[Mn_2(tolf)_4(bipyam)_2]$, **3**	3.67 (±0.13) × 10^6	3.67 (±0.13) × 10^{14}	4.26 (±0.16) × 10^6	0.99
$[Mn(tolf)_2(DMF)_2]_n$, **4**	3.28 (±0.18) × 10^5	3.28 (±0.18) × 10^{13}	4.29 (±0.19) × 10^5	0.99
HSA				
compound	K_{sv} (M^{-1})	k_q (M^{-1} s^{-1})	K (M^{-1})	n
Htolf[25]	6.10 (±0.38) × 10^4	6.10 (±0.38) × 10^{12}	3.12 (±0.25) × 10^5	0.63
$[Mn(tolf)_2(phen)(H_2O)]$, **1**	3.99 (±0.16) × 10^5	3.99 (±0.16) × 10^{13}	3.56 (±0.13) × 10^5	1.03
$[Mn_2(tolf)_4(py)_4(H_2O)]$, **2**	4.22 (±0.15) × 10^5	4.22 (±0.15) × 10^{13}	6.66 (±0.32) × 10^5	0.94
$[Mn_2(tolf)_4(bipyam)_2]$, **3**	1.02 (±0.04) × 10^6	1.02 (±0.04) × 10^{14}	9.04 (±0.39) × 10^5	1.02
$[Mn(tolf)_2(DMF)_2]_n$, **4**	7.80 (±0.34) × 10^5	7.80 (±0.34) × 10^{13}	5.88 (±0.22) × 10^5	1.01

through the bloodstream to cells and tissues.[71] Within this context, it is important to examine the interaction of potential drugs with SA; interaction with SA may reveal differentiated biological properties of the drug or novel transport pathways. The solutions of human serum albumin (HSA, bearing one tryptophan, Trp-214) and its extensively studied homologue bovine serum albumin (BSA, with two tryptophans, Trp-134 and Trp-212)) exhibit an intense fluorescence emission when excited at 295 nm, with $\lambda_{em,max}$ = 351 and 343 nm, respectively.[72] The addition of complexes **1**−**4** results in a quenching of the SA fluorescence emission which is usually attributed to subunit association, protein denaturation, substrate binding, or conformational changes of the protein.[73] Complexes **1**−**4** in buffer solution exhibit a maximum emission at 330 nm under the same experimental conditions (as also previously reported tolfenamato Zn(II) and Co(II) complexes),[25,26] and the SA fluorescence spectra have been corrected before the experimental data processing.

The significant fluorescence emission quenching as a result of the addition of complexes **1**−**4** to the BSA fluorescence signal at 343 nm as well as to the HSA fluorescence maximum at 351 nm (Figure 7) indicates the binding of each complex to the albumin and may be attributed to changes in tryptophan environment of SA because of possible changes in protein secondary structure.[73] The quenching constant values (k_q) for complexes **1**−**4** interacting with albumins have been calculated with the Stern−Volmer quenching equation (eq S1) and the corresponding Stern−Volmer plots (Figures S7 and S8) and are given in Table 1. These values indicate good SA quenching ability, and the k_q values of the complexes are higher than the corresponding values of free Htolf, with **3** exhibiting the highest quenching ability (k_q = 3.67 (±0.13) × 10^{14} M^{-1} s^{-1} for BSA and 1.02 (±0.04) × 10^{14} M^{-1} s^{-1} for HSA). The quenching constant (k_q > 10^{12} M^{-1} s^{-1}) has higher values than other compounds that quench the fluorescence of biopolymers (2.0 × 10^{10} M^{-1} s^{-1}), thus indicating the existence of a static quenching mechanism.[73]

The association binding constant (K) as well as the number of binding sites per albumin (n) for the complexes were calculated from the Scatchard equation (eq S2)[71] and the Scatchard plots (Figures S9 and S10), and the corresponding values are given in Table 1. The relatively high K values of all complexes are higher than those of free Htolf, with **2** having the highest K values for BSA (K = 4.32 × 10^6 M^{-1}) and **3** for HSA (K = 9.04 × 10^4 M^{-1}). A comparison of the association binding constants of the complexes for the albumins (K values) shows that almost all complexes (with the exception of **4**) present a higher binding strength for BSA than for HSA.

The value of the association constant of a compound to albumin should be in such a range that allows possible binding to, transfer by, and release from the albumins at its biological target. It should be noted that the binding constants of the complexes are lying in such a promising range. The values of K are high enough (3.56 × 10^5 to 4.32 × 10^6 M^{-1}), revealing the affinity of the complexes to bind to albumins; they are quite lower than the association constants of avidin to diverse ligands (K ≈ 10^{15} M^{-1}), which is among the strongest known

dx.doi.org/10.1021/ic4025487 | Inorg. Chem. 2014, 53, 2040−2052

Table 2. Spectral Features upon Addition of DNA (Band Studied in λ (nm), Percentage of Hyperchromism or Hypochromism ΔA (%), and Hypsochromism or Bathochromism $\Delta\lambda$ (nm)) and the DNA Binding Constants (K_b) of Complexes 1−4

compound	λ (nm) (ΔA (%)[a], $\Delta\lambda$ (nm)[b])	K_b (M^{-1})
Htolf[25]		5.00 (±0.10) × 10^4
$[Mn(tolf)_2(phen)(H_2O)]$, **1**	295 (+10, −8)	2.62 (±0.30) × 10^4
$[Mn_2(tolf)_4(py)_4(H_2O)]$, **2**	306 (−6.5, −4)	1.35 (±0.15) × 10^5
$[Mn_2(tolf)_4(bipyam)_2]$, **3**	312 (+7, −2)	2.65 (±0.17) × 10^5
$[Mn(tolf)_2(DMF)_2]$, **4**	298 (∼[c], ∼),	5.21 (±0.35) × 10^5
	310 (−5, ∼)	

[a]"+" denotes hyperchromism and "−" denotes hypochromism. [b]"+" denotes bathochromism and "−" denotes hypsochromism. [c]"∼" denotes "no significant change observed."

noncovalent interactions, revealing the possibility of release upon arrival to target tissues or cells.[73]

In relation to previously reported Co(II)[25] and Zn(II)[26] tolfenamato complexes, the quenching constants (k_q) for complexes **1**−**4** are more pronounced than for their Co(II) analogues and similar to those reported for Zn(II) tolfenamato complexes for both BSA and HSA, and the Mn(II) complexes **1**−**4** exhibit higher K values than the Zn(II) and Co(II) tolfenamato complexes reported.

3.5.3. Interaction with Calf-Thymus DNA. Metal complexes can interact with double-strand DNA in a covalent (replacement of at least one of its labile ligands by a DNA base) and/or a noncovalent way (intercalation due to $\pi \rightarrow \pi^*$ stacking interaction of the complex and DNA nucleobases, external electrostatic interaction as a result of Coulomb forces of metal complexes and the phosphate groups of DNA, or groove binding via van der Waals interaction or hydrogen bonding or hydrophobic bonding along the major or minor groove of DNA helix).[28,29,74] The tentative anticancer and anti-inflammatory activity of NSAIDs and their metal complexes could also be related to their DNA-binding ability;[18,19] thus, DNA-binding studies can be of significant interest, although their number with NSAIDs and their complexes was rather limited until now; e.g., complexes of oxicam NSAIDs intercalate to DNA[19] as well as a series of cobalt(II) and copper(II) complexes of carboxylate NSAIDs recently reported.[20,25−33]

UV spectroscopic titration experiments can provide useful information on the existing DNA-binding mode, with the appearance of hypochromism in the case of the intercalation and of a red shift (bathochromism) as evidence of stabilization of the DNA duplex being among the most predominant spectroscopic features.[75]

Complexes **1**−**4** exhibit similar behavior upon their addition to CT DNA solution. The UV spectra of DNA were recorded for a DNA concentration in the range 1.5 × 10^{-4} to 2.0 × 10^{-4} M at increasing mixing ratios r (= [complex]/[DNA]) (up to 0.3). The UV spectra of CT DNA in the presence of **1** at diverse r values are shown as an example in Figure S11. The intensity of the DNA band at λ_{max} = 258 nm exhibits a slight hypochromism with a red-shift of the λ_{max} up to 263 nm. These are the predominant features of the addition of the compounds in CT DNA solution and may be considered as evidence of a new adduct that the compounds form with double-helical CT DNA resulting in stabilization of the CT DNA duplex.[75,76]

The changes of the intense absorption bands (attributed to intraligand transitions of coordinated ligands[32,77]) in the UV spectra of compounds **1**−**4** (10^{-5} M) were studied after the addition of a CT DNA solution in diverse r values. These changes may give a first indication of the possible DNA-binding mode of each complex. For complex **4**, the addition of CT DNA in increasing amounts results in a 5% hypochromism of band I at 310 nm, while the intensity and the position of band II at 298 nm have no significant changes (Figure S12A). Similar is the behavior of complex **2** upon the addition of CT DNA (Figure S12B); i.e., the intensity of the band centered at 306 nm exhibits a decrease of 6.5% accompanied by a 4-nm blue-shift and the existence of an isosbestic point at 335 nm. In the UV spectrum of complex **3**, the band at 312 nm presents a 7% hyperchromism, and its intensity is gradually stabilized. These changes are accompanied by a slight blue-shift (up to 310 nm), and the existence of an isosbestic point at 333 nm (Figure S12C). Quite similar is the behavior of the intraligand transition band at 295 nm in the spectra of complex **1**, which shows a 10% hyperchromism and an 8-nm blue-shift (Table 2).

In most cases, a conclusion concerning the DNA-binding mode may not be safely extracted only by UV spectroscopic titration experiments. The existing data collected by the UV titration studies simply indicate binding of the compounds to CT DNA. Of course, the hypochromism observed for **2** and **4** may be considered evidence of a possible intercalative binding to DNA attributed to $\pi \rightarrow \pi^*$ stacking interactions; nevertheless, further experiments are necessary in order to clarify the binding mode.[77]

The DNA-binding constants of the compounds, K_b, were calculated via the Wolfe−Shimer equation[78] (eq S3) and the plots in Figure S13, and their values are given in Table 2. The K_b values are relatively high and in most cases are higher than that of free tolfenamic acid, suggesting that its coordination to Mn(II) results in a increase of the K_b value. The K_b values suggest a strong binding of the complexes to CT DNA, with complex **4** having the highest K_b value (= 5.21 (±0.35) × 10^5 M^{-1}) among the compounds, and close to the K_b value of the classical intercalator EB (= 1.23 (±0.07) × 10^5 M^{-1}) as calculated in ref 79. The K_b values of complexes **1**−**4** are similar to or lower than the corresponding Co(II)−tolfenamato complexes.[25]

The changes of DNA viscosity in the presence of a compound provide valuable information in the attempt to investigate and verify the DNA-binding mode of a compound, since DNA viscosity is very sensitive to DNA-length changes;[25,30] the relation between the relative solution viscosity (η/η_0) and DNA length (L/L_0) is given by the equation $L/L_0 = (\eta/\eta_0)^{1/3}$, where L_0 denotes the apparent molecular length in the absence of the compound.[32,77] In the case of partial or nonclassic intercalation to DNA (i.e., external groove binding or electrostatic interaction), the DNA helix is slightly bent or kinked, leading to a slight shortening of DNA length, and the DNA viscosity decreases slightly or remains unchanged.[32,75,80] In the case of classic intercalation, i.e. insertion of the compound in between DNA base pairs, the separation distance

dx.doi.org/10.1021/ic4025487 | Inorg. Chem. 2014, 53, 2040−2052

of the base pairs increases so that the compound may be hosted resulting in DNA lengthening and, subsequently, in an increase of DNA viscosity, the magnitude of which is proportional to the interaction strength.

Viscosity measurements of a CT DNA solution (0.1 mM) were performed after the addition of complexes **1**−**4** at increasing amounts (up to the value of r = 0.25; Figure 8). The

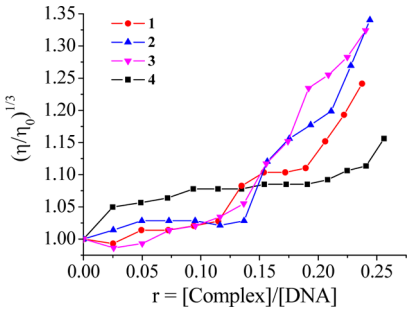

Figure 8. Relative viscosity $(\eta/\eta_o)^{1/3}$ of a buffer solution (150 mM NaCl and 15 mM trisodium citrate at pH 7.0) of CT DNA (0.1 mM) in the presence of complexes **1**−**4** in relation to the ratio [complex]/[DNA] (= r).

relative DNA viscosity (η/η_o) increases in the presence of all complexes; this increase is more pronounced in the case of complexes **2** and **3**, which present the higher K_b values as derived from UV spectroscopic studies (Table 2). In conclusion, the observed increase of the DNA viscosity in the presence of the tested compounds may serve as evidence of an intercalative DNA-binding mode,[25,30] a conclusion which completely enforces the preliminary findings from the UV spectroscopic studies.

EB (ethidium bromide = 3,8-diamino-5-ethyl-6-phenyl-phenanthridinium bromide) interacts with CT DNA via intercalation, which occurs via insertion of the planar EB phenanthridine ring in between adjacent base pairs on the DNA framework. The result of this intercalation is an intense fluorescence emission band which is due to the formation of the EB−DNA compound. Thus, EB is considered a typical indicator of intercalation when a DNA-intercalating compound is added into a solution of the EB−DNA compound, a quenching of the EB−DNA fluorescence emission may appear.[81] A DMSO solution of compounds **1**−**4**, when excited at 540 nm, does not present any appreciable fluorescence emission at room temperature and in the presence of DNA or EB. Therefore, the changes observed in the fluorescence emission spectra of an EB−DNA solution upon titration with the tested compounds may be used to study the EB-displacing ability of the compounds from the EB−DNA complex.[81]

The fluorescence emission spectra of pretreated EB-CT DNA have been recorded for [EB] = 20 μM and [DNA] = 26 μM with increasing amounts of each complex up to an r value of 0.45 (Figure 9A). The intensity of the emission band of the DNA-EB system at 592 nm decreases significantly upon the addition of complexes **1**−**4** (the final values are in the presence of the complexes up to 6−15% of the initial EB−DNA fluorescence emission intensity; Figure 9B). The observed high DNA−EB fluorescence emission quenching by the complexes is strong evidence of their significant EB-displacing ability and subsequently of probable intercalative interaction with CT DNA.[28−30]

The Stern−Volmer plots of EB−DNA fluorescence (Figure S14) illustrate the good agreement (R = 0.99) of the EB−DNA fluorescence quenching by the complexes with the linear Stern−Volmer equation (eq S4).[28−30] The Stern−Volmer constant values (K_{SV}) as obtained by the corresponding Stern−Volmer plots (Figure S14) suggest the tight binding of the complexes to DNA with **3** having the highest K_{sv} value (= 4.82 (±0.24) × 10^6 M^{-1}) among the compounds (Table 3). The K_{sv} values of complexes **1**−**4** are of the same magnitude as their Co(II)−tolfenamato analogues.[25]

Table 3. Percentage of EB−DNA Fluorescence Quenching (ΔI/Io, %) and Stern−Volmer Constants (K_{SV}) for Complexes 1−4

compound	EB−DNA fluorescence quenching (%)	K_{SV} (M^{-1})
Htolf[28]	74	1.15 (±0.04) × 10^6
[Mn(tolf)$_2$(phen)(H$_2$O)], **1**	92	8.54 (±0.56) × 10^5
[Mn$_2$(tolf)$_4$(py)$_4$(H$_2$O)], **2**	93	3.84 (±0.11) × 10^6
[Mn$_2$(tolf)$_4$(bipyam)$_2$], **3**	94	4.82 (±0.24) × 10^6
[Mn(tolf)$_2$(DMF)$_2$], **4**	85	3.78 (±0.16) × 10^5

4. CONCLUSIONS

The synthesis and the characterization of the novel neutral mono- and dinuclear and polymeric mangenese(II) complexes with the NSAID tolfenamic acid, the N-donor heterocyclic ligands 1,10-phenanthroline, pyridine, and 2,2′-bipyridylamine and/or the O-donor ligands H_2O and *N*,*N*-dimethylformamide

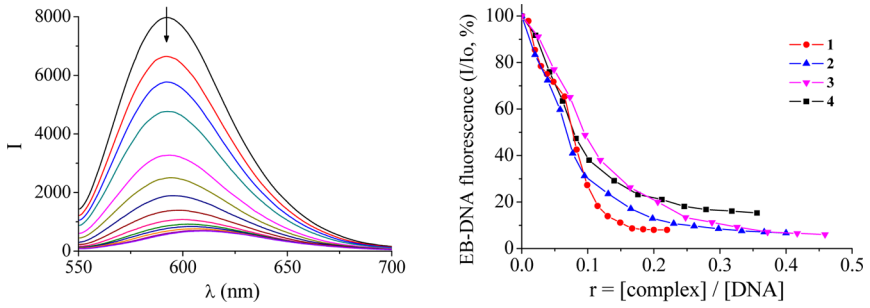

Figure 9. (A) Fluorescence emission spectra (λ_{exit} = 540 nm) of a buffer solution (150 mM NaCl, 15 mM trisodium citrate, pH 7.0) containing EB−DNA ([EB] = 20 μM, [DNA] = 26 μM) in the presence of increasing amounts of complex **2** (r = [complex]/[DNA] = 0−0.4). The arrow shows the changes observed upon the addition of **2**. (B) Plot of relative fluorescence emission intensity (%I/Io) at λ_{em} = 592 nm (λ_{exit} = 540 nm) of a buffer solution (150 mM NaCl and 15 mM trisodium citrate at pH 7.0) of EB−DNA in the presence of increasing amounts of complexes **1**−**4** in relation to the ratio [compound]/[DNA] (= r).

dx.doi.org/10.1021/ic4025487 | Inorg. Chem. 2014, 53, 2040−2052

have been achieved. The crystal structures of $[Mn(tolf)_2(phen)(H_2O)]$, $[Mn_2(\mu_2\text{-}H_2O)(\mu_2\text{-}tolf)_2(tolf)_2(py)_4]\cdot 1.5MeOH\cdot py$, $[Mn_2(\mu_2\text{-}tolf)_2(tolf)_2(bipyam)_2]$, and $[Mn(\mu_2\text{-}tolf)_2(DMF)_2]_n$ have been determined by X-ray crystallography, and the isolated products exhibit versatile coordination modes. In the mononuclear complex **1**, the tolfenamato ligands are displaying a combination of bidentate chelating and monodentate binding mode; in the dinuclear complex **2**, a combination of bidentate O,O′-bridging and a monodentate mode of the tolfenamato ligands exists, while in the dinuclear complex **3**, four tolfenamato ligands are bidentate with two of them being in a O,O′-bridging and two in O,O′-chelating mode. The tolfenamato ligands in the polymeric complex **4** are in the O,O′-bridging mode forming the basis of the polymeric network.

All complexes have been tested *in vitro* for free radical scavenging activity and soybean lipoxygenase inhibitory activity and were more active than free tolfenamic acid. The complexes exhibit low to moderate ability to scavenge DPPH radicals and significantly high scavenging activity against superoxide and hydroxyl radicals; they can also inhibit significantly the activity of soybean lipoxygenase. Complex **1** is the most active radical scavenger and the most potent LOX inhibitor.

The tested compounds show high quenching ability of the BSA and HSA fluorescence and tight binding affinity for the albumins providing relatively high binding constants ($K = 3.56 \times 10^5$ to 4.32×10^6 M^{-1}), which are in the optimum range to allow the binding, the transfer, and the release upon arrival at the targets. Complexes **1**−**4** exhibit higher quenching constants than their corresponding Co(II)−tolfenamato analogues and similar to the Zn(II) ones while their SA-binding constants are the highest among the metal−tolfenamato complexes studied.[25,26]

UV spectroscopic titration studies, DNA-viscosity measurements, and fluorescence experiments were employed to investigate the binding of the complexes CT DNA. The DNA-binding strength of the complexes was evaluated with UV spectroscopic titrations with $[Mn(\mu_2\text{-}tolf)_2(DMF)_2]_n$ exhibiting the highest K_b ($K_b = 5.21\ (\pm 0.35) \times 10^5$ M^{-1}) value among the compounds examined, which is on the same order as the K_b value of EB. Competitive binding studies with EB revealed the significant ability of the tested compounds to displace the well-known intercalator EB from the EB−CT DNA complex, suggesting intercalation as the most possible DNA-binding mode, a binding mode that was further confirmed by DNA-viscosity experiments after the addition of the compounds.

The reported albumin binding studies may be considered as a first means to evaluate the binding of the complexes to serum proteins; these studies may be expanded to more serum proteins. The results of the antioxidant activity of the complexes are promising since the complexes are more active than the reference compounds such as trolox and caffeic acid, and their potential anti-inflammatory ability should be further investigated. The ability of the reported compounds to act as DNA intercalators may open a new window for their use as potential metallodrugs.

■ ASSOCIATED CONTENT

Supporting Information

Tables S1−S6, Figures S1−S6, and CIF files giving crystallographic data for complexes **1**−**4**. Table S7 containing the antioxidant activity data and Figures (S7−S14) containing the plots and equations (S1-S4) used for the quantitative assessment of the interaction studies with BSA, HSA, and DNA. This material is available free of charge via the Internet at http://pubs.acs.org. CCDC 947340−947343 contain the supplementary crystallographic data for this paper. These data can be obtained free of charge via www.ccdc.cam.ac.uk/conts/retrieving.html (or from the Cambridge Crystallographic DataCentre, 12 Union Road, Cambridge CB21EZ, U. K.; fax: (+44) 1223−336−033 or e-mail: deposit@ccde.cam.ac.uk).

■ AUTHOR INFORMATION

Corresponding Author

*Tel.: +30 + 2310997790. Fax: +30 + 2310997738. E-mail: gepsomas@chem.auth.gr.

Notes

The authors declare no competing financial interest.

■ ACKNOWLEDGMENTS

This research has been cofinanced by European Social Fund (ESF) and Greek national funds (National Strategic Reference Framework (NSRF): Archimides III). Financial support from the Slovenian Research Agency (ARRS) through project P1-0175 is gratefully acknowledged. This project was also supported by EU COST Action CM1105.

■ REFERENCES

(1) Larson, E. J.; Pecoraro, V. L. In *Manganese Enzymes*; Pecoraro, V. L., Ed.; VCH Publishers Inc: New York, 1992.

(2) Mullins, C. S.; Pecoraro, V. L. *Coord. Chem. Rev.* **2008**, *252*, 416−443.

(3) Kessissoglou, D. P. *Coord. Chem. Rev.* **1999**, *186*, 837−858.

(4) Guo, Z.; Sadler, P. J. *Angew. Chem., Int. Ed.* **1999**, *38*, 1512−1531.

(5) Dorkov, P.; Pantcheva, I.; Sheldrick, W.; Figge, H.; Petrova, R.; Mitewa, M. *J. Inorg. Biochem.* **2008**, *102*, 26−32.

(6) Zampakou, M.; Akrivou, M.; Andreadou, E. G.; Raptopoulou, C. P.; Psycharis, V.; Pantazaki, A. A.; Psomas, G. *J. Inorg. Biochem.* **2013**, *121*, 88−99.

(7) Li, M.; Chen, C.; Zhang, D.; Niu, J.; Ji, B. *Eur. J. Med. Chem.* **2010**, *45*, 3169−3177.

(8) Zhou, D.; Chen, Q.; Qi, Y.; Fu, H.; Li, Z.; Zhao, K.; Gao, J. *Inorg. Chem.* **2011**, *50*, 6929−6937.

(9) Chen, X.; Tang, L.; Sun, Y.; Qiu, P.; Liang, G. *J. Inorg. Biochem.* **2010**, *104*, 1141−1147.

(10) Singh, D. P.; Kumar, K.; Sharma, C. *Eur. J. Med. Chem.* **2010**, *45*, 1230−1236.

(11) Duffy, C. P.; Elliott, C. J.; O'Connor, R. A.; Heenan, M. M.; Coyle, S.; Cleary, I. M.; Kavanagh, K.; Verhaegen, S.; O'Loughlin, C. M.; NicAmhlaoibh, R.; Clynes, M. *Eur. J. Cancer* **1998**, *34*, 1250−1259.

(12) Amin, A. R.; Vyas, P.; Attur, M.; Leszczynskapiziak, J.; Patel, I. R.; Weissmann, G.; Abramson, S. B. *Proc. Natl. Acad. Sci. U.S.A.* **1995**, *92*, 7926−7930.

(13) Kim, K.; Yoon, J.; Kim, J. K.; Baek, S. J.; Eling, T. E.; Lee, W. J.; Ryu, J.; Lee, J. G.; Lee, J.; Yoo, J. *Biochem. Biophys. Res. Commun.* **2004**, *325*, 1298−1303.

(14) Smith, M.; Hawcroft, G.; Hull, M. A. *Eur. J. Cancer* **2000**, *36*, 664−674.

(15) Klampfer, L.; Cammenga, J.; Wisniewski, H. G.; Nimer, S. D. *Blood* **1999**, *93*, 2386−2394.

(16) Inoue, A.; Muranaka, S.; Fujita, H.; Kanno, T.; Tamai, H.; Utsumi, K. *Free Radic. Biol. Med.* **2004**, *37*, 1290−1299.

(17) Barbaric, M.; Kralj, M.; Marjanovic, M.; Husnjak, I.; Pavelic, K.; Filipovic-Grcic, J.; Zorc, D.; Zorc, B. *Eur. J. Med. Chem.* **2007**, *42*, 20−29.

(18) Zhang, T.; Otevrel, T.; Gao, Z.; Gao, Z.; Ehrlich, S. M.; Fields, J. Z.; Boman, B. M. *Cancer Res.* **2001**, *61*, 8664−8667.

(19) Roy, S.; Banerjee, R.; Sarkar, M. *J. Inorg. Biochem.* **2006**, *100*, 1320−1331.

(20) Tsiliki, P.; Perdih, F.; Turel, I.; Psomas, G. *Polyhedron* **2013**, *53*, 215−222.
(21) Weder, J. E.; Dillon, C. T.; Hambley, T. W.; Kennedy, B. J.; Lay, P. A.; Biffin, J. R.; Regtop, H. L.; Davies, N. M. *Coord. Chem. Rev.* **2002**, *232*, 95−126.
(22) Moilanen, E.; Kankaanranta, H. *Pharmacol. Toxicol.* **1994**, *75* (Suppl. II), 60.
(23) Kovala-Demertzi, D.; Kourkoumelis, N.; Koutsodimou, A.; Moukarika, A.; Horn, E.; Tiekink, E. R. T. *J. Organomet. Chem.* **2001**, *620*, 194−201.
(24) Kovala-Demertzi, D.; Galani, A.; Demertzis, M. A.; Skoulika, S.; Kotoglou, C. *J. Inorg. Biochem.* **2004**, *98*, 358−364.
(25) Tsiliou, S.; Kefala, L.; Perdih, F.; Turel, I.; Kessissoglou, D. P.; Psomas, G. *Eur. J. Med. Chem.* **2012**, *48*, 132−142.
(26) Tarushi, A.; Totta, X.; Raptopoulou, C. P.; Psycharis, V.; Psomas, G.; Kessissoglou, D. P. *Dalton Trans.* **2012**, *41*, 7082−7091.
(27) Psomas, G.; Kessissoglou, D. P. *Dalton Trans.* **2013**, *42*, 6252−6276.
(28) Dimiza, F.; Fountoulaki, S.; Papadopoulos, A. N.; Kontogiorgis, C. A.; Tangoulis, V.; Raptopoulou, C. P.; Psycharis, V.; Terzis, A.; Kessissoglou, D. P.; Psomas, G. *Dalton Trans.* **2011**, *40*, 8555−8568.
(29) Dimiza, F.; Papadopoulos, A. N.; Tangoulis, V.; Psycharis, V.; Raptopoulou, C. P.; Kessissoglou, D. P.; Psomas, G. *Dalton Trans.* **2010**, *39*, 4517−4528.
(30) Dimiza, F.; Papadopoulos, A. N.; Tangoulis, V.; Psycharis, V.; Raptopoulou, C. P.; Kessissoglou, D. P.; Psomas, G. *J. Inorg. Biochem.* **2012**, *107*, 54−64.
(31) Tarushi, A.; Kastanias, F.; Psycharis, V.; Raptopoulou, C. P.; Psomas, G.; Kessissoglou, D. P. *Inorg. Chem.* **2012**, *51*, 7460−7462.
(32) Tolia, C.; Papadopoulos, A. N.; Raptopoulou, C. P.; Psycharis, V.; Garino, C.; Salassa, L.; Psomas, G. *J. Inorg. Biochem.* **2013**, *123*, 53−65.
(33) Tarushi, A.; Karaflou, Z.; Kljun, J.; Turel, I.; Psomas, G.; Papadopoulos, A. N.; Kessissoglou, D. P. *J. Inorg. Biochem.* **2013**, *128*, 85−96.
(34) *CrysAlis PRO*; Agilent Technologies: Yarnton, England, 2011.
(35) Sheldrick, G. M. *SHELXS-97: Program for Crystal Structure Determination*; University of Göttingen: Göttingen, Germany, 1997.
(36) Sheldrick, G. M. *SHELXL-97: Program for the Refinement of Crystal Structures*; University of Göttingen: Göttingen, Germany, 1997.
(37) Kontogiorgis, C.; Hadjipavlou-Litina, D. *J. Enzyme Inhib. Med. Chem.* **2003**, *18*, 63−69.
(38) Re, R.; Pellegrini, N.; Proteggente, A.; Pannala, A.; Yang, M.; Rice-Evans, C. *Free Radical Biol. Med.* **1999**, *26*, 1231−1237.
(39) Prabhakar, K. R.; Veerapur, V. P.; Bansal, P.; Kumar, V.; Reddy, M.; Barik, A.; Reddy, B. K.; Reddanna, P.; Priyadarsini, K. I.; Unnikrishnan, M. K. *Bioorg. Med. Chem.* **2006**, *14*, 7113−7120.
(40) Viossat, V.; Lemoine, P.; Dayan, E.; Dung, N.; Viossat, B. *Polyhedron* **2003**, *22*, 1461−1470.
(41) Wang, J.; Ping, L.; Chen, Y.; Liu, Z. *Acta Crystallogr., Sect. E* **2004**, *60*, m628−m630.
(42) Xuan, X.; Zhao, P. *Acta Crystallogr., Sect. E* **2007**, *63*, m3180−m3181.
(43) Caneschi, A.; Ferraro, F.; Gatteschi, D.; Melandri, M. C.; Rey, P.; Sessoli, R. *Angew. Chem., Int. Ed. Engl.* **1989**, *28*, 1365−1367.
(44) Coucouvanis, D.; Reynolds, R. A., III; Dunham, W. R. *J. Am. Chem. Soc.* **1995**, *117*, 7570−7571.
(45) Ye, B.; Mak, T.; Williams, I. D.; Li, X. *Chem. Commun.* **1997**, 1813−1814.
(46) Reynolds, R. A., III; Dunham, W. R.; Coucouvanis, D. *Inorg. Chem.* **1998**, *37*, 1232−1241.
(47) Gomez, V.; Corbella, M. *Eur. J. Inorg. Chem.* **2009**, 4471−4482.
(48) Skyrianou, K. C.; Perdih, F.; Papadopoulos, A. N.; Turel, I.; Kessissoglou, D. P.; Psomas, G. *J. Inorg. Biochem.* **2011**, *105*, 1273−1285.
(49) Mukherjee, P. S.; Min, K. S.; Arif, A. M.; Stang, P. J. *Inorg. Chem.* **2004**, *43*, 6345−6350.
(50) Gomez, V.; Corbella, M.; Font-Bardia, M.; Calvet, T. *Dalton Trans.* **2010**, *39*, 11664−11674.
(51) Palanisami, N.; Murugavel, R. *Inorg. Chim. Acta* **2011**, *365*, 430−438.
(52) Iikura, H.; Nagata, T. *Inorg. Chem.* **1998**, *37*, 4702−4711.
(53) Milios, C. J.; Kefalloniti, E.; Raptopoulou, C. P.; Terzis, A.; Escuer, A.; Vicente, R.; Perlepes, S. P. *Polyhedron* **2004**, *23*, 83−95.
(54) Baruah, A. M.; Karmakar, A.; Baruah, J. B. *Open Inorg. Chem. J.* **2008**, *2*, 62−68.
(55) Tangoulis, V.; Psomas, G.; Dendrinou-Samara, C.; Raptopoulou, C. P.; Terzis, A.; Kessissoglou, D. P. *Inorg. Chem.* **1996**, *35*, 7655−7660.
(56) Das, M. C.; Bharadwaj, P. K. *J. Am. Chem. Soc.* **2009**, *131*, 10942−10949.
(57) Xu, Y.; Tang, W. *Z. Kristallogr.—New Cryst. Struct.* **2010**, *225*, 543−545.
(58) Guo, F.; Zhu, B.; Zhang, X.; Song, Y.; Wu, P. *J. Coord. Chem.* **2010**, *63*, 1130−1138.
(59) It was not possible to perform the variable temperature magnetic measurements for complex **4** since its quantity was not sufficient. For more details, see the Experimental Section.
(60) Cini, R.; Giorgi, G.; Cinquantini, A.; Rossi, C.; Sabat, M. *Inorg. Chem.* **1990**, *29*, 5197−5200.
(61) Borgstahl, G. E. O.; Pokross, M.; Chehab, R.; Sekher, A.; Snell, E. H. *J. Mol. Biol.* **2000**, *296*, 951−959.
(62) Rackova, L.; Oblozinsky, M.; Kostalova, D.; Kettmann, V.; Bezakova, L. *J. Inflammation* **2007**, *4*, 15 Article No.
(63) Young, R. N. *Eur. J. Med. Chem.* **1999**, *34*, 671−685.
(64) van der Zee, J.; Eling, T. E.; Mason, R. P. *Biochemistry* **1989**, *28*, 8363−8367.
(65) Bukhari, S. B.; Memon, S.; Tahir, M. M.; Bhanger, M. I. *J. Mol. Struct.* **2008**, *892*, 39−46.
(66) Pontiki, E.; Hadjipavlou-Litina, D.; Chaviara, A. T.; Bolos, C. A. *Bioorg. Med. Chem. Lett.* **2006**, *16*, 2234−2237.
(67) Liu, Z.; Wang, B.; Yang, Z.; Li, Y.; Qin, D.; Li, T. *Eur. J. Med. Chem.* **2009**, *44*, 4477−4484.
(68) Christidis, P. C.; Georgousis, Z. D.; Hadjipavlou-Litina, D.; Bolos, C. A. *J. Mol. Struct.* **2008**, *872*, 73−80.
(69) El-Gammal, O. A.; Abu El-Reash, G. M.; Ghazy, S. E.; Radwan, A. H. *J. Mol. Struct.* **2012**, *1020*, 6−15.
(70) Pontiki, E.; Hadjipavlou-Litina, D. *Bioorg. Med. Chem.* **2007**, *15*, 5819−5827.
(71) Lakowicz, J. R. *Principles of Fluorescence Spectroscopy*, 3rd ed.; Springer: New York, 2006.
(72) Wang, Y.; Zhang, H.; Zhang, G.; Tao, W.; Tang, S. *J. Lumin.* **2007**, *126*, 211−218.
(73) Rajendiran, V.; Karthik, R.; Palaniandavar, M.; Stoeckli-Evans, H.; Periasamy, V. S.; Akbarsha, M. A.; Srinag, B. S.; Krishnamurthy, H. *Inorg. Chem.* **2007**, *46*, 8208−8221.
(74) Kljun, J.; Bratsos, I.; Alessio, E.; Psomas, G.; Repnik, U.; Butinar, M.; Turk, B.; Turel, I. *Inorg. Chem.* **2013**, *52*, 9039−9052.
(75) Long, E. C.; Barton, J. K. *Acc. Chem. Res.* **1990**, *23*, 271−273.
(76) Pyle, A. M.; Rehmann, J. P.; Meshoyrer, R.; Kumar, C. V.; Turro, N. J.; Barton, J. K. *J. Am. Chem. Soc.* **1989**, *111*, 3053−3063.
(77) Koumousi, E. S.; Zampakou, M.; Raptopoulou, C. P.; Psycharis, V.; Beavers, C. M.; Teat, S. J.; Psomas, G.; Stamatatos, T. C. *Inorg. Chem.* **2012**, *51*, 7699−7710.
(78) Wolfe, A.; Shimer, G.; Meehan, T. *Biochemistry* **1987**, *26*, 6392−6396.
(79) Dimitrakopoulou, A.; Dendrinou-Samara, C.; Pantazaki, A. A.; Alexiou, M.; Nordlander, E.; Kessissoglou, D. P. *J. Inorg. Biochem.* **2008**, *102*, 618−628.
(80) Garcia-Gimenez, J. L.; Gonzalez-Alvarez, M.; Liu-Gonzalez, M.; Macias, B.; Borras, J.; Alzuet, G. *J. Inorg. Biochem.* **2009**, *103*, 923−934.
(81) Dhar, S.; Nethaji, M.; Chakravarty, A. R. *J. Inorg. Biochem.* **2005**, *99*, 805−812.